Hierarchically Structured, All-Aqueous-Coated Hydrophobic Surfaces with pH-Selective Droplet Transfer Capability

Jordan Brito[1], Kaustubh Asawa[2], Alexander Marin,[3] Alexander K. Andrianov,[3] Chang-Hwan Choi[2], and Svetlana A. Sukhishvili[1]**

[1]Department of Materials Science & Engineering, Texas A&M University, College Station, TX 77843, USA

[2]Department of Mechanical Engineering, Stevens Institute of Technology, Hoboken, NJ 07030, USA

[3]Institute for Bioscience and Biotechnology Research, University of Maryland, Rockville, MD 20850, USA

KEYWORDS: self-assembly, layer-by-layer, hydrophobicity, surface morphology, microstructure, fluorination

Abstract

Often inspired by nature, techniques for precise droplet manipulation have found applications in microfluidics, microreactors, and water harvesting. However, a widely applicable strategy for surface modification combining simultaneous hydrophobicity and pH-sensitivity has not yet been achieved by employing environmentally friendly assembly conditions. The introduction of pH-

responsive groups to an otherwise fluorinated polyphosphazene unlocks pH-selective droplet capture and transfer. Here, an all-aqueous layer-by-layer (LbL) deposition of polyelectrolytes is used to create unique hydrophobic coatings endowing surfaces with the ability to sense environmental pH. The high hydrophobicity of these coatings (ultimately reaching a contact angle >120° on flat surfaces) is enabled by the formation of hydrophobic nanoscale domains and controllable by degree of fluorination of polyphosphazenes, polyamine binding partner, deposition pH, and coating thickness. Inspired by the hierarchical structure of rose petals, these versatile coatings reach a contact angle >150° when deposited on structured surfaces while introducing a tunable adhesivity that enables precise droplet manipulation. The films exhibited a strongly pronounced parahydrophobic rose petal behavior characterized through the contact angle hysteresis. Depositing as few as five bilayers (~25 nm) on microstructured rather than smooth substrates resulted in superhydrophobicity with water contact angles >150° and the attenuation of the contact angle hysteresis, enabling highly controlled transfer of aqueous droplets. The pH-selective droplet transfer was achieved between surfaces with either the same microstructure and LbL film building blocks which were assembled at different pH, or between surfaces with different microstructures coated with identical films. The demonstrated capability of these hydrophobic LbL films to endow surfaces with controlled hydrophobicity through adsorption from aqueous solutions and control the adhesion and transfer of water droplets between surfaces can be used in droplet-based microfluidics applications and water collection/harvesting.

Introduction

Surfaces with programmable droplet adhesion have propelled technology in both fundamental research and applications,[1] such as droplet-based reactions in microfluidics, precise sensing and analysis in lab-on-a-chip systems, and efficient fog harvesting.[2–7] Research in droplet manipulation typically employs external stimuli,[8] including magnetic,[9–11] electric,[12,13] acoustic,[14,15] and photo-actuation.[16–18] However, these approaches rely on the stimulus application, droplet functionality, or involve active handling, and thus have limitations for autonomous, self-guided environmental applications. In contrast, surfaces that can 'recognize' droplet environments (acidity or presence of chemicals), and autonomously 'act', *i.e.*, adjust droplet adhesiveness in response to the environment, are self-regulated, do not require power sources, and are more suitable for autonomous operation and monitoring of reactions in the droplets or in applications for water harvesting.

Several approaches were developed that enable autonomous droplet manipulation based on droplet pH, which are based on a combination of hydrophobic, pH-responsive surface chemistry with hierarchical nano- and microstructures.[19–24] However, in many of these instances, the approaches are synthetically challenging and not easily applicable to arbitrary surfaces, such as in the cases of pH-responsive species grafted onto the surfaces of nanostructures. Furthermore, droplet manipulation using soft surfaces, such as polydimethylsiloxane (PDMS), remained unexplored, despite their importance for microfluidic and biomedical devices. In these cases, the use of layer-by-layer (LbL) deposition to apply uniform, conformal coatings to complex surfaces is a simple, yet highly effective, bottom-up approach to modulate surface wettability.[25–29] However, LbL assemblies of polyelectrolyte multilayers have not been previously considered as suitable candidates for controlling droplet adhesion and transfer, because LbL films of typical

water-soluble polymers have contact angles below 90°[30–32] and thus do not support formation of easily transferable water droplets.

Built by sequential adsorption of oppositely charged polyelectrolytes from aqueous solutions, LbL films display properties that depend on the chemical nature of polyelectrolyte components and also on interlayer interactions which can be tuned by polyelectrolyte charge density[33,34], salt concentration[35,36], and in the case of weak polyelectrolytes – solution pH[37–39]. Yet, the ionic groups that aid the solubility of the polyelectrolytes also impart an intrinsic hydrophilicity to the surface assemblies. In prior work, wettability of LbL films could be tuned only within a small range of contact angles by varying pH or polyelectrolyte concentration, while the films remained hydrophilic.[25,26,29] Superhydrophobicity could be only achieved with LbL films using incorporation of hydrophobically modified nanoparticles, non-aqueous deposition of fluorinated polycations, and/or further chemical modification of LbL surfaces.[28,40–42] However, to the best of our knowledge, as-deposited all-aqueous polyelectrolyte multilayer films have never before achieved highly controllable hydrophobicity that guides droplet formation and transfer.

A major roadblock in using LbL films for pH-sensitive droplet manipulation is the difficulty in achieving simultaneously surface hydrophobicity and variable ionization of assembled polymers. To overcome this, polyphosphazenes (PPZs), with exceptional synthetic flexibility owing to their unique backbone chemistry, were synthesized with both fluorinated and carboxylic acid side groups.[43] Previous work from our group includes investigating the hydrophobicity of LbL films formed by fluorinated PPZs of different fluorination degrees[44] and nature of the ionic groups.[45] The hydrophobic fluorinated PPZs composing these films have been shown to be biocompatible,[44,46] enabling future applications of these coatings to biomedical devices. Also important, the mild, all-aqueous conditions used for self-assembly of polyelectrolyte multilayers

present an important environmentally friendly alternative to the harsh assembly conditions needed for traditional superhydrophobic surfaces.[47]

Herein, we report a facile approach to tune the hydrophobicity of PPZ-based LbL coatings within a wide range of contact angles solely by altering the all-aqueous deposition conditions. By depositing the hydrophobic LbL coatings conformally on micropatterned surfaces, we amplify the hydrophobicity of the coating to the Cassie-Baxter wetting state while maintaining a controllable degree of droplet adhesivity where the droplet is in contact with the coatings. We show that aqueous assembly of ionic fluorinated PPZs results in a spontaneous formation of a hierarchical surface structure (with nanoscale domains arising from LbL deposition on microscale patterns of the underlying laser lithographed substrate) which, together with pH-responsiveness of the deposited films, enable controlling surface hydrophobicity and adhesivity for precise droplet manipulation.

RESULTS AND DISCUSSION

Controlling the Morphology of Polyelectrolyte Multilayer Films via Assembly Conditions

The goal of this research is to construct hydrophobic coatings from all-aqueous solutions that can be applied to virtually any surface *via* a LbL technique. This technique is enabled by the fact that PPZ copolymers containing trifluoroethoxy and carboxylatophenoxy side groups (FPs, Fig. 1A) remain water soluble, even up to 77% trifluoroethoxy substitution, until the anionic charges are neutralized within the LbL coating. To achieve this goal, first, the effects of polyanion and polycation binding partner on the hydrophobicity of the LbL film were explored. Fig. 1A illustrates the LbL procedure for forming polyelectrolyte multilayers from polyamines with

varying chemistry and substitution at the amino group (poly(vinylamine hydrochloride) (PVAm), poly(allylamine hydrochloride) (PAH), branched polyethyleneimine (BPEI), poly(L-lysine hydrobromide) (PLL), and poly(diallyldimethylammonium chloride) (PDADMAC)) and water-soluble anionic PPZs with varying degrees of fluorination (PCPP [0% of trifluoroethoxy groups], FP60 [60%], and FP77 [77%]). Notably, FP60 and FP77 were water-soluble for the tested pHs ranging from 4 to 6, despite their high degree of fluorination. However, PCPP was insoluble below pH 6.5. Therefore, coatings of PVAm with FP60 and FP77, denoted $(PVAm/FPx)_5$, where 5 is the number of bilayers, were assembled at pH 5 on flat silicon substrates, while the $(PVAm/PCPP)_5$ films were assembled at pH 6.5. Because increased fluorine content is expected to increase hydrophobicity of the polymer and decrease the dielectric constant,[48] an increase in CA with increasing fluorination was expected. This trend was observed in our experiments (Fig. 1B), where the advancing CA of coatings containing PPZs with 0% fluorination, *i.e.*, $(PVAm/PCPP)_5$ was ~45°, whereas the advancing CA of $(PVAm/FP77)_5$ coatings reached ~130°. However, the receding angle for all samples on flat silicon were ~0°, demonstrating a highly adhesive property of the multilayer films. With higher fluorination, the films were also more compact (Fig. S1), consistent with previous results from our group that also reported more linear film growth and lower swelling ratios.[44,46,49] Films of FP*x* constructed with another polyamine (*i.e.*, homopolypeptide PLL) displayed similar wetting and growth behavior (Fig. S2). Consistently, FP77-based coatings had not only the highest hydrophobicity of the FP's but also the highest reported CA of all-aqueous assembly of polyelectrolyte multilayers to our knowledge. Thus, we selected FP77 for further experiments and investigated the effect of polyamine binding partner.

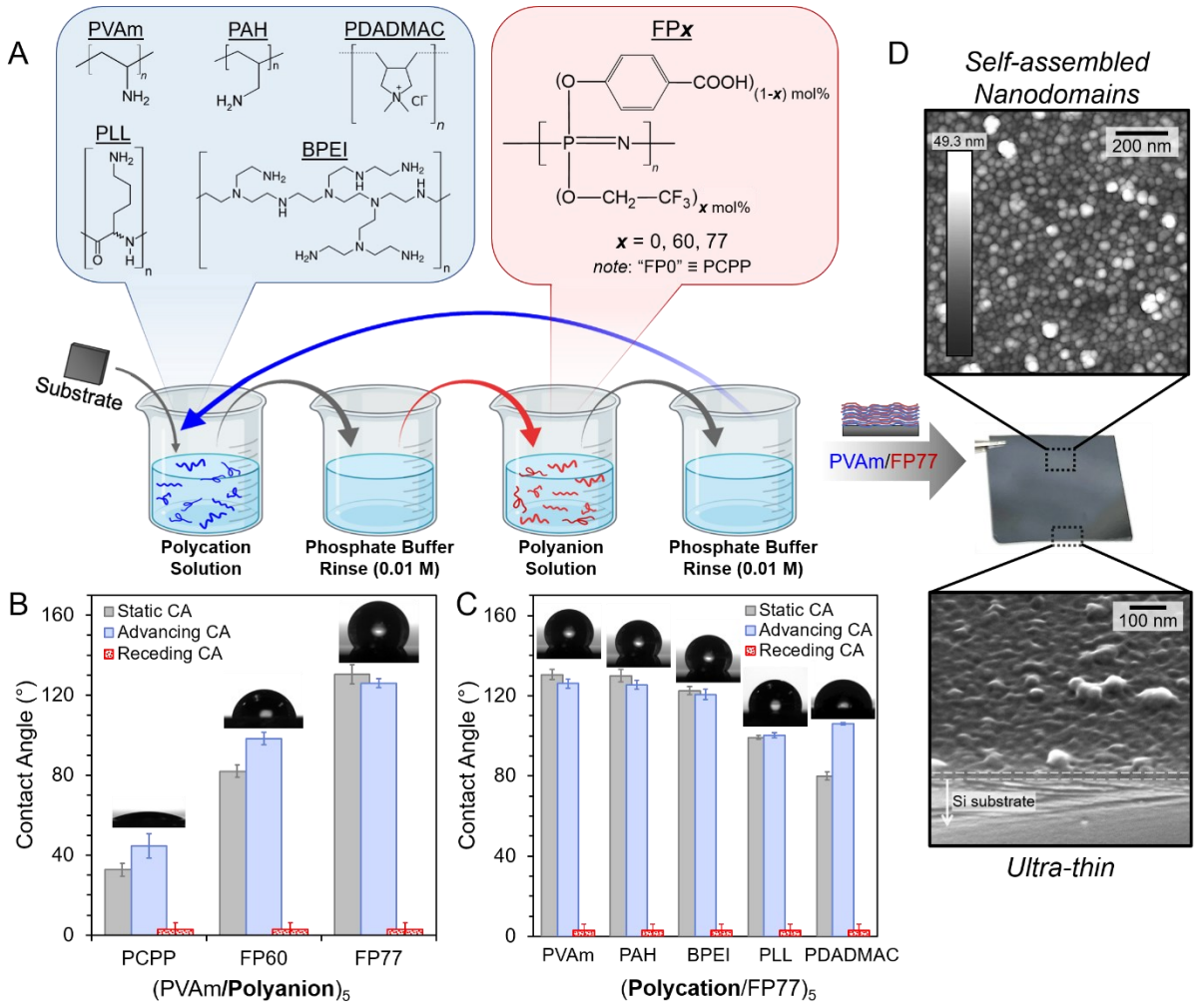

Figure 1. (A) Schematic representation of procedure for the deposition of polycation/FP*x* layer-by-layer (LbL) coatings from all-aqueous solutions. (B,C) Apparent contact angles of 5-bilayer coatings with varied polyanion fluorination degree (B) and varied polycation partner (C). Inset optical images show ~7 μL water droplets on 5-bilayer LbL coatings. (D) Morphology (top) and thickness (bottom) of a $(PVAm/FP77)_5$ coating on a flat silicon substrate shown using AFM and SEM, respectively.

Polyamines with different types of amino groups were then used as polycation partners to determine the effect of steric hinderance in ionic pairing on coating hydrophobicity. Fig. 1C shows

that PVAm and PAH, both containing primary, sterically unhindered amines, formed films with similar static CAs ~130° when assembled from solutions at pH 5. BPEI, containing 25% of primary, 25% of tertiary, and 50% of secondary amino groups, caused a ~10° decrease in static CA, and PLL, with butyl spacers between the primary amines and the backbone, displayed further ~20°-reduced hydrophobicity. Lastly, coatings formed with PDADMAC, containing quaternary ammonium groups known to cause the largest steric hindrance in ionic pairing,[36,50,51] along with greater backbone distance between charges, showed the lowest static CA of ~80°, allowing easier access of water into the film. Interestingly, however, the advancing CA of the PDADMAC coatings was ~106°, which was significantly higher than the static CA. The difference is likely due to weak ionic pairing within the film, resulting in higher mobility of PDADMAC.[36,52] The surface that contacts the droplet allows facile reorientation of hydrophilic groups to the surface, becoming more hydrophilic than the surface that is not contacting the droplet, yet is reversible after exposure to air.[53] Such chemical heterogeneity across the droplet contact line increases pinning and hence creates a difference between the static and advancing CA. This rapid surface reorientation is demonstrated in Fig. S3. In contrast, such surface reorientation was inhibited in the films with strong ionic pairing between primary amino groups of PVAm or PAH and carboxylate moieties of PPZs.[51] Note that all assemblies had similar thicknesses after depositing five bilayers (Fig. S4), eliminating the effect of film thickness on their resulting contact angles. Previously, in experiments with more hydrophilic LbL films of differently sterically hindered polyamines and polystyrene sulfonate, the dependence of CA on the strength of interpolymer binding of the multilayer films was attributed to adjacent layer interpenetration.[54] Here we show for the first time that the CA of highly hydrophobic LbL films can be controlled directly through the strength of ionic pairing *via* direct assembly of water-soluble hydrophobic PPZs.

It should be noted that the static CAs of FP77-containing multilayer coatings (~130°) were significantly higher than those reported for a spun-cast film of a 100% fluorinated PPZ, poly[bis(2,2,2-trifluoroethoxy)phosphazene] (PTFEP), recorded as 104°.[55] The high CAs of PVAm/FP77 films are attributed to the nanoscale roughness R (defined as the ratio of the actual surface area to the area of a 2D projection of the surface) created by the domains, as shown in Fig. 1D. The nanodomains likely originate from the microphase separation of hydrophobic groups of FPs within the coating that are further stabilized by the ionically paired polyelectrolytes. This roughness resulted in an increase in the apparent CA, θ_W, according to the Wenzel equation[56] $\cos\theta_W = R\cos\theta_Y$, where θ_Y is the Young's CA on a smooth surface.

Because all FPs used in this work were weak polyelectrolytes (*i.e.*, contained ionizable carboxylic groups), we then studied the occurrence and size of the nanodomains as a function of the pH of assembly solutions. Through image analysis of atomic force microscopy (AFM) images (Fig. 2A-C; see also Fig. S5) we found that while the average domain size was almost independent of the film assembly conditions (pH between 4 and 6), the root-mean-square (RMS) roughness was the highest at pH 5. The fact that RMS roughness for the films assembled at pH 4 and 6 was approximately the same, but their CAs were significantly different (Fig. 2D) suggests that the roughness itself could not explain the difference in CAs.

To test a hypothesis that the decrease in CA for the films assembled at pH 6 was caused by enhanced ionization of FPs, we explored the ionization state of carboxylic groups of FPs in LbL films using attenuated total reflectance-Fourier transform infrared (ATR-FTIR) spectroscopy. In Fig. 2E, spectra from ~100-nm-thick PVAm/FP77 coatings (to increase the sensitivity) assembled from solutions at varied pH were compared with the spectra of drop-cast neat film components to identify peaks and quantify the ionization degree of carboxylic groups. In the PVAm/FP77 spectra,

the ratio of the intensities of the peak at 1552 cm^{-1} and the broad shoulder at 1700 cm^{-1} (associated with asymmetric COO^- stretching and carbonyl stretching, respectively) were quantified and used to calculate the ionization degree at each pH shown in Fig. 2F (see Fig. S6 for an example of calculation). At pH 4, many carboxylic groups within the films are left unionized, while at pH 6, most groups are ionized. The apparent pK_{app} of FP77 within the multilayers, as estimated from the data in Fig. 2F, was around 4 – lower than the pK_{app} of FP77 in solution (~5.6, Fig. S7), which has been reported for other weak polyacids in multilayer films.[57] Taken together, the AFM and FTIR results point to the reasons for the changes in CA observed on PVAm/FP77 coatings assembled at different pH values: while the average lateral size of the domains was almost constant, and the RMS roughness changed only slightly with pH, a drastic decrease in CA by 20° between pH 5 and 6 (Fig. 2D) is due to enhanced ionization of assembled FP77. Because the film deposition is controlled by the balance of electrostatic charges,[58] the higher charge density on FP77 at a higher deposition pH also led to a lower ratio of strongly bound deposited FP77 to PVAm (Fig. S8). Similar pH dependences of the CA were also seen in assemblies with other polycations, *i.e.*, BPEI and PDADMAC (Fig. S9).

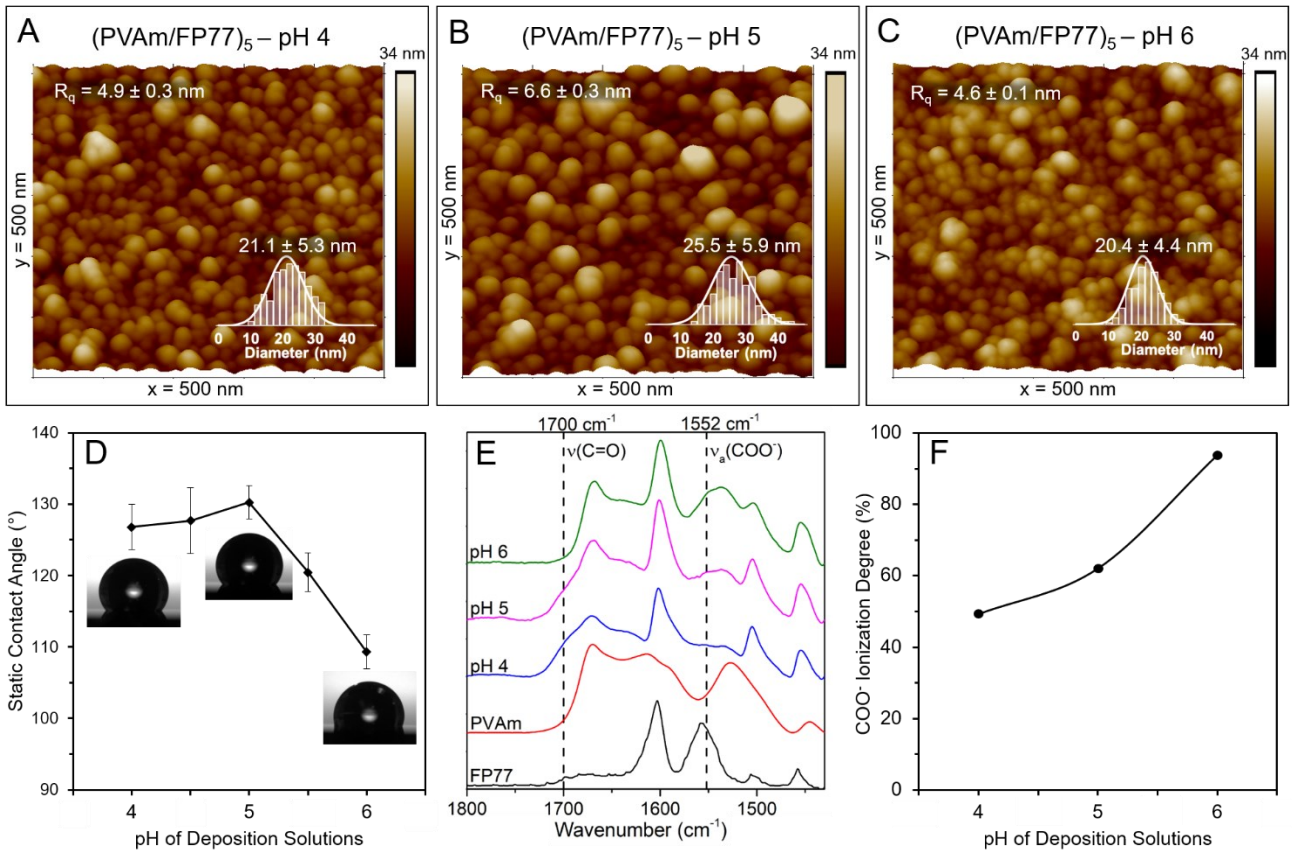

Figure 2. AFM 3D micrographs of $(PVAm/FP77)_5$ films deposited from pH 4 (A), pH 5 (B), and pH 6 (C). RMS roughness, average feature diameter, and distributions of feature diameters are shown as insets in the AFM images. (D) Static contact angle for $(PVAm/FP77)_5$ coatings deposited from solutions at pH 4 to 6. Optical images show water droplets on $(PVAm/FP77)_5$ coatings at pH 4, 5, and 6. (E) ATR-FTIR spectra of drop-cast FP77 and PVAm, and 100-nm-thick PVAm/FP77 films deposited from solutions at pH 4, 5, and 6. Spectra are overlaid with arbitrary offset for clarity. (F) Ionization degree of FP77 carboxylic groups in 100-nm-thick PVAm/FP77 coatings deposited from solutions at pH 4 to 6.

While the surface morphology and CA data in Fig. 2 were collected with films of similar thickness (23-26 nm as measured by ellipsometry, Fig. S10), a question arises of the effect of film

thickness on surface wettability. To study this effect, PVAm/FP77 coatings were assembled with up to 9 bilayers and their surface morphology and CA were analyzed. The RMS roughness was obtained by analysis of AFM 3D micrographs (Figs. 3A-C) and feature diameters from 2D AFM images (Fig. S11). Fig. 3D shows that both the RMS roughness and feature diameter increased with coating thickness. In agreement with the Wenzel theory, the apparent CA increased from 90° for one-bilayer to 140° for nine-bilayer coatings, gradually leveling off with increasing thickness (Fig. 3E). Scanning electron microscopy (SEM) images of the prime layer, third bilayer, and fifth bilayer also elucidate a gradual formation of the surface morphology with coating thickness (Fig. S12). We propose that these features are initially formed due to preaggregation in solution, shown by supramolecular assembly of a similar fluorinated PPZ.[59] These features are likely further enhanced at the surface after neutralization of charge within the LbL films. Fig. S13 shows that for FP77 assemblies with another polycation (BPEI), a similar trend was observed. The data in Fig. 3 show that the CA of a $(PVAm/FP77)_5$ coating can be further increased from 120° to 138° through deposition of an additional four bilayers, which leads to an increase in the feature size of the phase-separated domains. Because the thickness of LbL coatings is easily and precisely controllable, a wide range of wetting properties are now achievable with these fluorinated PPZ LbL systems due to the thickness dependence of the surface morphology and coating hydrophobicity.

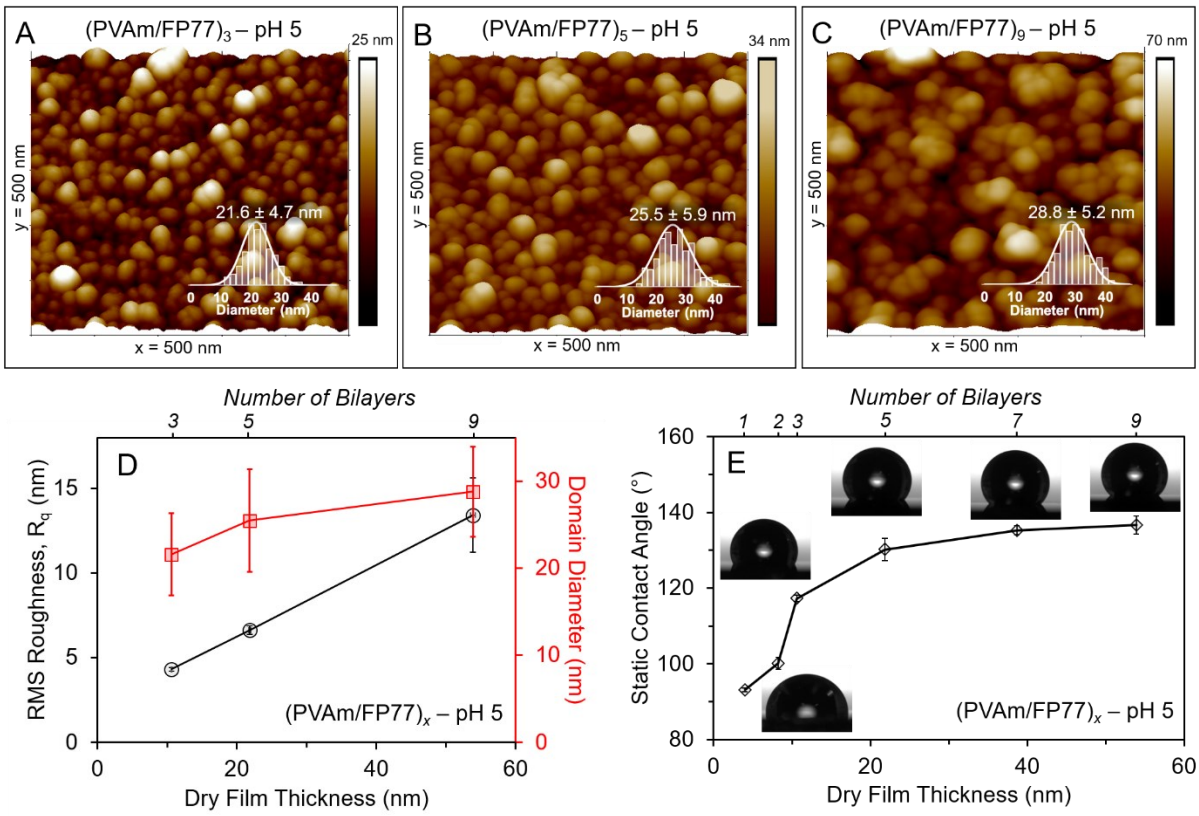

Figure 3. (A,B,C) AFM 3D micrographs of PVAm/FP77 LbL coatings with 3 bilayers (A), 5 bilayers (B), and 9 bilayers (C) deposited from pH 5 solutions. Distributions of feature diameters are shown as inset on the AFM micrographs. (D) RMS roughness and domain diameters collected from the provided AFM micrographs. (E) Static contact angle of PVAm/FP77 LbL coatings of varied thickness deposited from pH 5.

Coating Patterned Surfaces for Droplet Manipulation

In addition to high CA, PVAm/FP77 coatings deposited on flat silicon substrates showed high contact angle hysteresis (CAH >120°, determined by the difference between the advancing and receding CAs; see Fig. 1C), demonstrating highly adhesive properties. To achieve droplet manipulation, however, surface adhesiveness should be controlled at a lower level. To that end,

we used micro- and nanopatterned silicon rather that flat silicon substrates for PVAm/FP77 coating deposition. In this approach, the hydrophobicity of the coated surfaces is amplified to a Cassie-Baxter-like superhydrophobic state with tunable CAH based on the solid fraction of surface in contact with a droplet or the deposition pH. The Cassie-Baxter state is defined by the retention of air underneath the droplet, creating a composite interface with the surface, and the apparent CA in the Cassie-Baxter state, θ_{CB}, is described by $\cos\theta_{CB} = R\varphi\cos\theta_Y + \varphi - 1$, where φ is the fraction of the solid-liquid interface and defined by the fraction of raised surface area to the total area.[60]

In Fig. 4A, SEM images of $(PVAm/FP77)_5$ coatings on microstructured silicon demonstrate their conformality on all exposed surfaces, including between ridges on grooved wafers and on the randomly etched needles of black silicon. The grooved silicon wafers used in these studies provide a reliable comparison across samples because the dynamic CA measurements taken perpendicular to the groove direction minimize distortions from droplet pinning caused by structure edges.[61] Grooved silicon wafers with solid fractions φ = 0.8, 0.5, and 0.2 were coated and their advancing and receding CAs were compared to flat silicon (φ = 1) and black silicon (φ < 0.1). Initially, all bare silicon surfaces had a CA ~ 0° after cleaning with UV treatment and sulfuric acid. The $(PVAm/FP77)_5$ coatings increased the static CA >150° on all patterned silicon. Furthermore, as shown in Fig. 4B, the receding CA of the grooved silicon increased with decreased solid fraction due to reduced contact between the droplet and the adhesive LbL coating. The coated black silicon, with needle-like structures and the lowest solid fraction (φ < 0.1), resulted in the most hydrophobic surface, displaying a CA ~170°, CAH <3°, and roll-off angle <1°. Precisely tunable CAH was achievable by coating strategic surface structures ranging from flat silicon (CAH >130°) and microscale grooves (30° < CAH < 120°) to nanoscale pillars and needles (CAH <3°). The surfaces

appeared more hydrophobic with decreasing solid fraction (φ), as shown in optical images in Fig. 4C, agreeing with the Cassie-Baxter relationship between φ and θ_{CB}. Additionally, the coating thickness does not affect the initial solid fraction in the case of microscale structures, while it does in the case of nanoscale structures (Fig. S14).

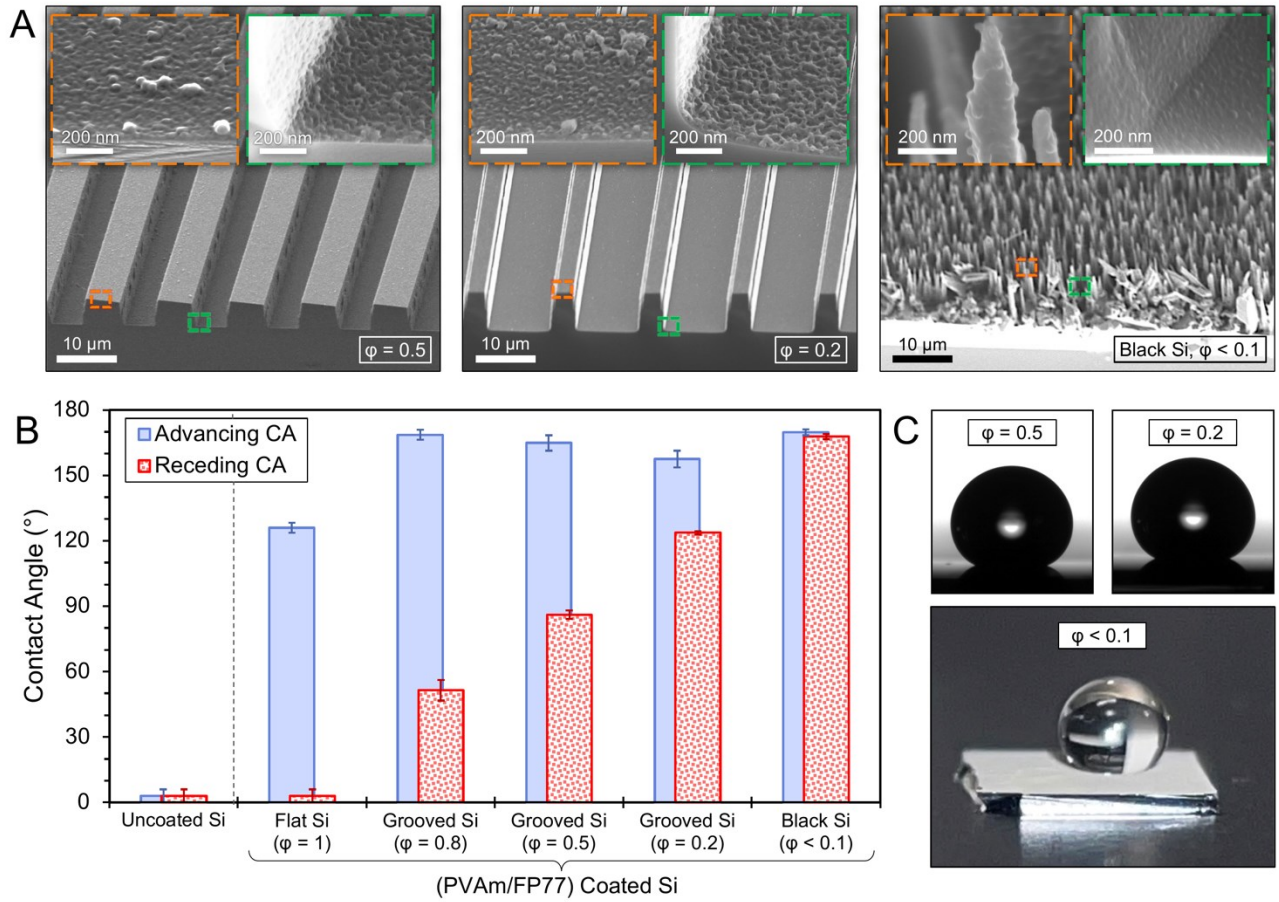

Figure 4. (A) Scanning electron microscopy images of (PVAm/FP77)-coated grooved silicon with 50% solid fraction (φ = 0.5), 20% solid fraction (φ = 0.2), and 'black silicon' with <10% solid fraction (φ < 0.1), from left to right. Insets show magnification of PVAm/FP77 coatings on high (orange) and low (green) areas of the structured silicon wafers. (B) Apparent contact angles for uncoated and (PVAm/FP77)-coated silicon wafers with varied solid fractions (φ = 1 [flat], 0.8

[grooved], 0.5 [grooved], 0.2 [grooved], or <0.1 [black Si]). Contact angles for all uncoated silicon wafers were ~0°. (C) Optical images show a water droplet on each sample.

The tunable CAH and hence the droplet retention force[61] based on surface structures enabled a controlled droplet transfer between wafers depending on the difference between the CAH of the wafer holding the droplet and the wafer receiving the droplet. As shown in Fig. 5A, with the grooved silicon samples with the coating of $(PVAm/FP77)_5$, a successful droplet transfer exhibits no-loss transfer of the entire water droplet from the donor wafer to the top, receiving wafer. An unsuccessful transfer may either exhibit partial or no transfer between wafers. As expected, all grooved silicon wafers were able to transfer water droplets away from coated black silicon because of the lower CAH (*i.e.*, droplet retention force) of the black silicon than the coated grooved silicon. Additionally, this necessary combination of low CAH on the bottom donor wafer and high CAH on the receiving wafer for successful droplet transfer was also demonstrated between the grooved silicon samples with varying solid fractions (Fig. 5B, see Supporting video S1). In the case of transfer between $\varphi = 0.2$ and $\varphi = 0.5$ and transfer between $\varphi = 0.5$ and $\varphi = 0.8$, the difference in hysteresis on the donor and receiving wafers were similar, yet the transfer between $\varphi = 0.2$ and $\varphi = 0.5$ was 74% successful while the transfer between $\varphi = 0.5$ and $\varphi = 0.8$ was 0% successful (see Supporting video S2). This result also highlights the necessity for a low CAH specifically on the donor wafer. Furthermore, all experimental combinations with the donor wafer with higher φ (*i.e.*, higher CAH) on the bottom were 0% successful, reinforcing the importance of a CAH gradient between wafers.

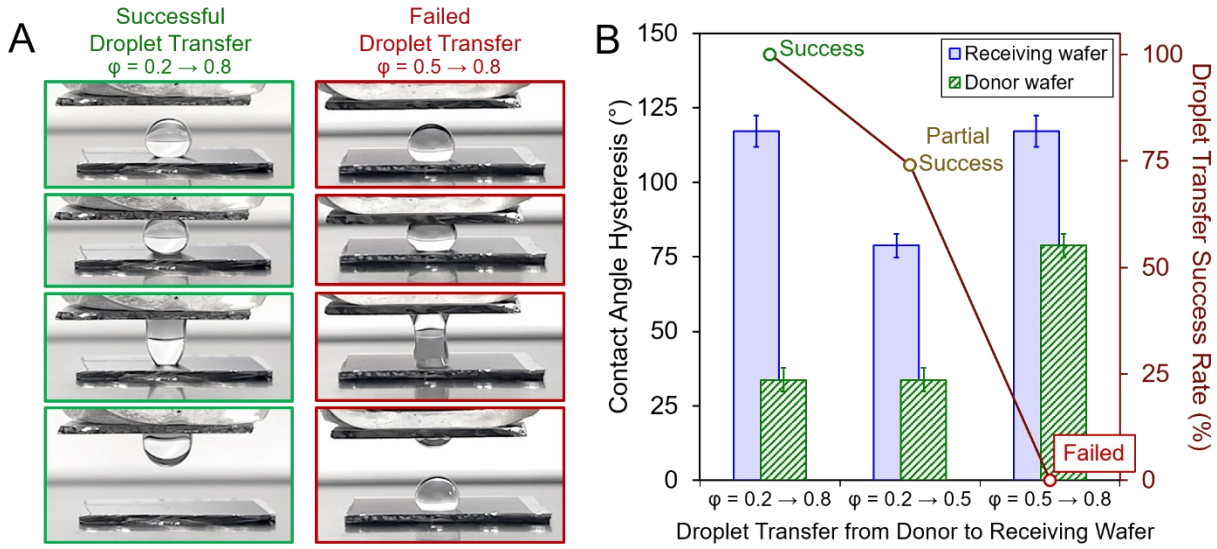

Figure 5. (A) Differences in contact angle hysteresis and droplet transfer success rate between $(PVAm/FP77)_5$-coated grooved silicon samples with solid fractions φ = 0.8, 0.5, and 0.2. (B) Images of failed (left) and successful (right) droplet transfer between $(PVAm/FP77)_5$-coated grooved silicon samples. Ultrapure water at pH 7 was used for all measurements.

In addition to the structure-induced control over the CAH, we sought to achieve a control of CAH via changes in assembly conditions (pH) of the deposited coatings. Fig. 6A shows that CAH, using ultrapure water, for the coatings deposited on grooved silicon (φ = 0.2) decreases with deposition pH. The decrease in advancing CA is likely due to increased ionization of FP77 and thus easier wetting of the coating assembled at higher pH values. This trend was also observed for grooved silicon with a higher solid fraction (φ = 0.5, see Fig. S15).

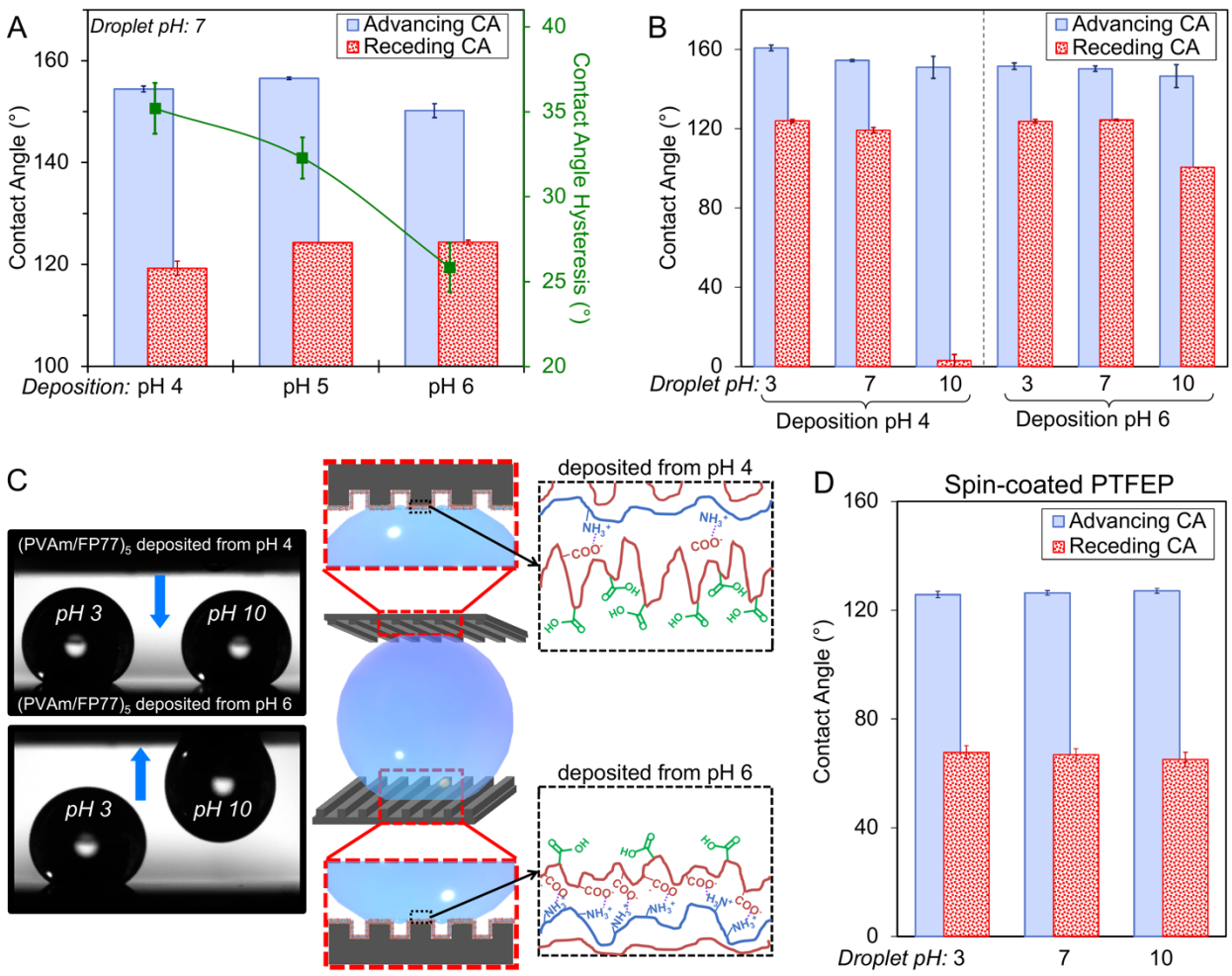

Figure 6. (A) Apparent contact angles and contact angle hysteresis using ultrapure water (pH 7) for coated, grooved silicon [$(PVAm/FP77)_5$ on $\varphi = 0.2$] are shown as a function of deposition pH. (B) Apparent contact angles for $(PVAm/FP77)_5$ coated, grooved silicon ($\varphi = 0.2$) deposited from pH 4 and 6 using ultrapure water adjusted to pH 3, 7, and 10. (C) Optical images show an alkaline water droplet (pH 10) selectively transferring from the bottom wafer to the top wafer, while the acidic water droplet (pH 3) remains. Top and bottom wafers are both grooved silicon ($\varphi = 0.2$) coated with $(PVAm/FP77)_5$, while the top wafer is deposited from pH 4 and the bottom from pH 6. Illustration shows the proposed mechanism of this pH-responsive droplet adhesion based on deposition pH. (D) Apparent contact angles for spin-coated poly[bis(2,2,2-

trifluoroethoxy)phosphazene] (PTFEP) on flat silicon using ultrapure water adjusted to pH 3, 7, and 10.

By taking advantage of the fact that LbL assemblies of weak polyelectrolytes are highly responsive to pH,[62] we aimed to achieve further control of droplet transfer through selective response of PVAm/FP77 coatings to changes in the droplet pH. We hypothesized that due to higher hydrophilicity and water adhesiveness of carboxylate groups in comparison with neutral carboxylic acid groups,[24,63] coatings deposited at different pH will be able to demonstrate distinct CAHs for droplets of varied acidity. To test this hypothesis, we deposited $(PVAm/FP77)_5$ coatings on grooved silicon ($\varphi = 0.2$) from solution at pH 4 and pH 6 and studied the dependence of apparent CAs on droplet pH (Fig. 6B, see Supporting video S3). It should be noted that the coatings were stable in the experimental pH range, from pH 3 to pH 10. As expected, the coating deposited from pH 4 was more adhesive to basic droplets (pH 10) because of a lowered receding CA. This pH-responsive adhesiveness was used to selectively transport a basic (pH 10) droplet away from the coating deposited from pH 6 (at the bottom of Fig. 6C images) using the coating deposited from pH 4 (at the top of Fig. 6C images), while the acidic (pH 3) droplet remained. The schematics in Fig. 6C show how such a behavior was programmed at the step of coating deposition: when deposited at pH 6, few pH-responsive groups are exposed to the surface because many of the carboxylate groups on the FP77 capping layer are paired electrostatically within the LbL coating. However, when deposited at pH 4, fewer carboxylic acid groups are ionized and paired electrostatically, leaving many pH-responsive groups exposed to the surface. The difference in number of electrostatically unpaired carboxylic acid groups enabled the coating deposited from pH 4 to be more ionized, and thus more hydrophilic, when exposed to basic droplets than the acidic

droplets. To highlight the novelty of the combined hydrophobicity and pH sensitivity of the PVAm/FP77 coatings, a comparison was made with spin-coated PTFEP on a flat silicon wafer. In addition to lacking solubility in water, PTFEP, containing no ionizable groups, was shown to have no change in CAH with droplet pH (Fig. 6D), demonstrating the importance of harnessing both pH-dependent ionizable groups and hydrophobic groups at the surface.

Applications and Durability of $(PVAm/FP77)_5$ Coatings

The $(PVAm/FP77)_5$ coatings were also applied to microgrooved PDMS substrates to demonstrate their viability in PDMS-based microfluidic devices. The successful coating of PDMS was confirmed using a simple dye test, as the polar groups in the LbL coatings were expected to retain a Rhodamine 5G dye while the uncoated PDMS did not change in appearance (Fig. S16). However, in contrast to the negatively charged silicon oxide groups formed on the surface of silicon, untreated PDMS does not have specific charged groups on the surface, so the priming layer was assumed to be held by non-electrostatic binding on the PDMS surface. As shown in Fig. 7A, a comparison of the advancing and receding CA for bare and coated flat PDMS ($\varphi = 1$) and microgrooved PDMS ($\varphi = 0.8$, 0.5, and 0.2) samples revealed an expansion in the CAH for coated samples primarily caused by a reduced receding CA. The reduction in receding CA with higher φ is attributed to the higher area of contact between the coating and the water droplet. It should be noted that the coated, flat PDMS displayed a lower advancing CA and a higher receding CA than coated flat silicon, which could be a result of a sparser deposited coating caused by weaker binding of the priming layer, leaving some areas of PDMS exposed. Yet, these surfaces also enable successful or failed droplet transfer depending on the difference in CAH (Fig. 7B, see Supporting video S4 and S5, respectively). This tunable adhesive property of the coatings may be

advantageous in applications requiring manipulation of singular droplets. In Fig. 7C, we show that coated, grooved PDMS with φ = 0.5 can transfer a 4 μL aqueous droplet containing iron(III) chloride ($FeCl_3$) from coated, grooved PDMS with φ = 0.2 to combine with an aqueous droplet containing sodium thiocyanate (NaSCN). This reaction produces an aqueous droplet containing iron(III) thiocyanate complex ions ($FeSCN^{2+}$), and resulting in a no-loss droplet-based reaction (see Supporting video S6). This demonstration shows that the coatings deposited on a micro-grooved PDMS substrate can be used for precise capture and transfer of aqueous droplets for controlled mixing of droplets with largely varied cargo and performing chemical reactions in controllably adhered droplets. We also envision that these surfaces may be used for passive collection of products from microreactors/reactions-in-droplets, as they can selectively release droplets based on droplet pH.

The broad applicability of the coatings is further demonstrated in Fig. 7D-F, in which the PVAm/FP77 coatings are applied to various substrates, including bio-relevant materials such as titanium, glass, and fabrics. Fig. 7F shows that the ultrathin coatings also retain the original optical properties of the underlying surface. To demonstrate the adhesion of the coating to the underlying substrates, three subsequent tape tests were performed on the same area of a 15-bilayer coating (made thicker for clarity in optical microscope imaging). The coating showed high adhesion to the substrate and retained hydrophobicity even after three cycles of testing (Fig. S17). Furthermore, the solvent resistance of the coatings was assessed by changes in thickness and static CA. The coatings showed good resistance to nonpolar solvents (toluene and hexanes), maintaining both the original thickness and static CA of the coating (Fig. S18). As the main applications of this coating are in aqueous environments, the coatings were tested under aqueous flow conditions, demonstrating that the thickness and CA of the coatings do not change even after 5 minutes under

a jet of water (30 mL/s, Fig. S19). Altogether, these robust ultrathin coatings can be applied to virtually any surface with strong adhesion to endow the surface with hydrophobic and pH-responsive properties enabling intrinsic pH-sensing abilities for selective droplet transfer.

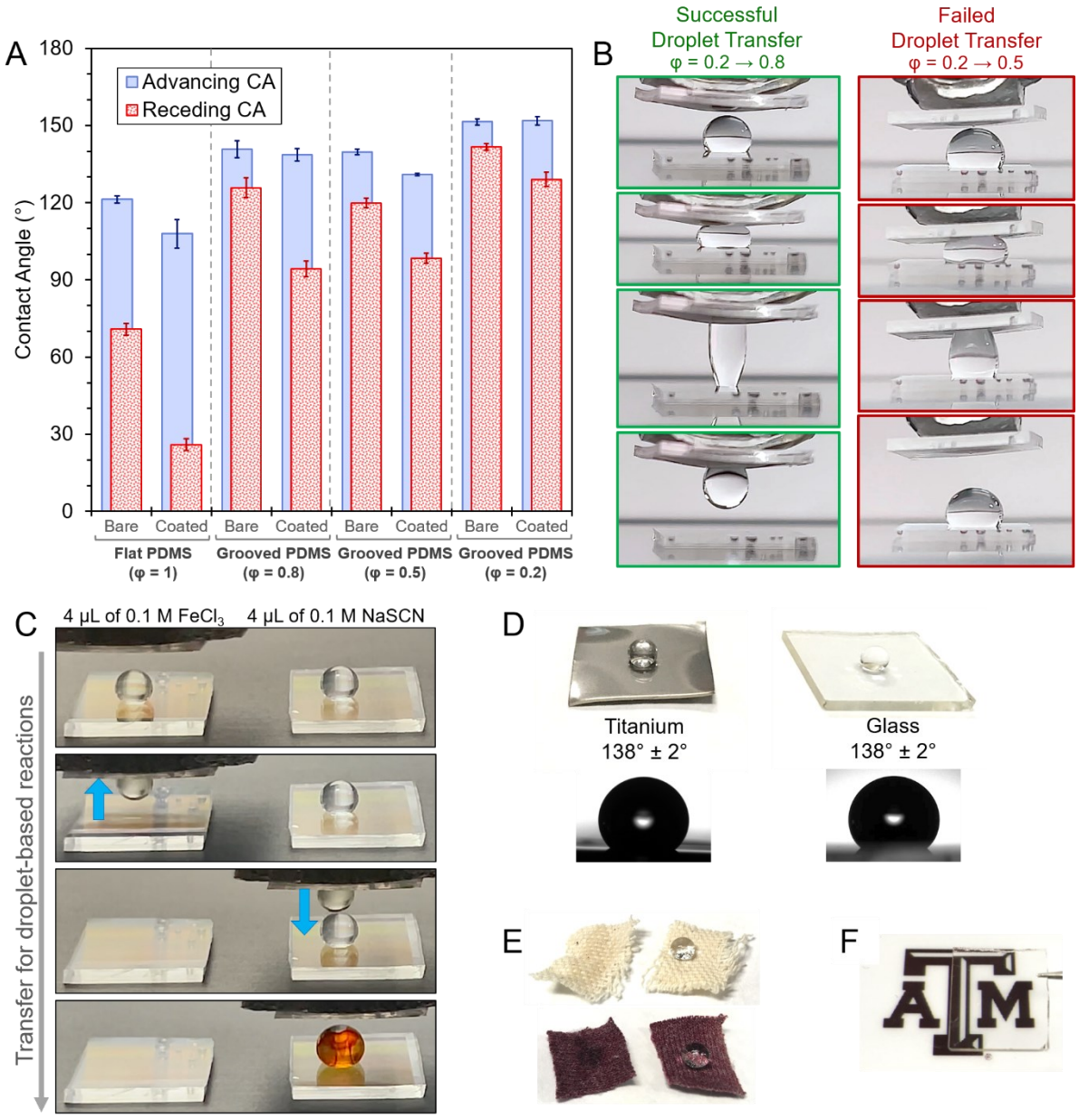

Figure 7. (A) Advancing and receding contact angles for uncoated and $(PVAm/FP77)_5$-coated PDMS samples with varied solid fractions (φ = 1 [flat], 0.8 [grooved], 0.5 [grooved], or 0.2 [grooved]). (B) Images of successful (left) and failed (right) droplet transfer between coated PDMS

samples. Optical images demonstrating $(PVAm/FP77)_5$ coating versatility and applications: (C) Transference of a 4 μL 0.1 M $FeCl_3$ droplet between coated, grooved PDMS ($\varphi = 0.2 \rightarrow 0.5$) to combine with a 4 μL 0.1 M NaSCN droplet; (D) water contact angles on coated titanium sheet and glass; (E) water droplets on uncoated (left) and coated (right) cotton and polyester fabrics; and (F) retained transparency of coated glass.

Conclusions

In summary, we have demonstrated a highly versatile, all-aqueous strategy to design hydrophobic surfaces with controlled contact angle hysteresis, allowing for precise droplet manipulation with pH sensitivity. Using a layer-by-layer assembly of fluorinated, ionic polyphosphazenes with polyamines, we created highly hydrophobic surfaces with hierarchical nanodomains that could be applied to virtually any substrate. The PVAm/FP77 LbL coatings form pH-dependent, self-assembled domains *via* phase segregation of the hydrophobic trifluoroethoxy moieties, imparting a controllable nanoscale architecture to their surface. The seemingly incompatible properties of all-aqueous deposition and high hydrophobicity result from the PPZs' combination of ionic carboxylatophenoxy groups with high degrees of trifluoroethoxy groups, maintaining water solubility while allowing for the unique self-assembly of highly hydrophobic, ultrathin coatings with controllable adhesivity.

For achieving controlled droplet transfer, the hysteresis behavior can be precisely controlled by depositing the films from different solution pH or on patterned surfaces with varied solid fraction. Based on structural differences, the contact angle hysteresis could be tuned between <3° (very low droplet adhesion) and >130° (very high droplet adhesion). Additionally, the pH-responsive behavior of the carboxylic acid groups on FP77 imparts a pH-selective droplet adhesion to the surface. The coatings are highly adhesive to the substrate and are stable in an aqueous

environment over a wide range of pH, aqueous flow conditions, and nonpolar solvents. The additional mechanical robustness makes them suitable for potential applications in droplet-based microfluidics, lab-on-a-chip, reaction-in-a-droplet, and fog harvesting technologies.

EXPERIMENTAL SECTION

Materials

All chemicals used to prepare the multilayer films were used as received. Sodium phosphate monobasic dihydrate, branched polyethyleneimine (BPEI, M_w = 750 kDa), poly(allylamine hydrochloride) (PAH, M_w = 50 kDa), poly(diallyldimethylammonium chloride) (PDADMAC, M_w = 400-500 kDa; 20 wt. % in water), and hydrochloric acid were purchased from Sigma-Aldrich. Poly(vinylamine hydrochloride) (PVAm, M_w = 25 kDa) and poly(L-lysine hydrobromide) (PLL, M_w = 120 kDa) were purchased from Polysciences, Inc. Sodium hydroxide and sulfuric acid were purchased from VWR. Silicon wafers (University Wafer, Inc., <100> orientation, P/B doped, 0–100 Ohm-cm resistivity) were used as substrates for multilayer deposition unless otherwise specified. Ultrapure Milli-Q water (Merck Millipore) with a resistivity of 18.2 MΩ/cm was used in all experiments. Poly[bis(2,2,2-trifluoroethoxy)phosphazene] (PTFEP) and ionic polyphosphazenes with a fluorination degree of 0% (PCPP, M_w = 800 kDa), 60% (FP60, M_w = 246 kDa), and 77% (FP77, M_w = 200 kDa) were synthesized as reported previously.[43,44,64] For the reaction-in-a-droplet demonstration, sodium thiocyanate (VWR) and iron(III) chloride (VWR) were used as received. For solvent resistance testing, ethanol (200 proof, Sigma-Aldrich), methanol (ACS grade, VWR), dimethyl sulfoxide (ACS grade, VWR), toluene (anhydrous, 99.8%, Alfa Aesar), and hexanes (ACS grade, Sigma-Aldrich) were used as received.

Fabrication of Micro-patterned Silicon and PDMS Wafers

Polished silicon wafers (University Wafer, Inc.) were cleaned in piranha solution (mixture of H_2SO_4 and H_2O_2 in 3:1 in volume), rinsed with deionized water, and dehydrated on a hotplate at 100°C for 10 min. A positive photoresist (PR1-1000A, Futurrex, Inc., Franklin, NJ) was spin-coated on a wafer for 40 s at 3000 rpm, resulting in a film thickness of 1 μm, and baked on a hotplate at 120°C for 2 min. The photoresist layer was then exposed through a photomask of specific micropatterns using a mask aligner (Karl Suss MA6) with a soft contact mode for a total dosage of 70 mJ/cm^2. The registered pattern on the photoresist layer was then developed in resist developer (RD6, Futurrex, Inc., Franklin, NJ) for 30 s, rinsed in water for 5 min, and dried in N_2 gas for 5 min. The photoresist pattern was then transferred onto a silicon wafer by etching using a cryogenic deep reactive ion etching (DRIE) process (PlasmaLab 100, Oxford Instruments, Bristol, UK) at -100°C using SF_6 and O_2 gases. The flow rates of the gases were 30 and 20 sccm for SF_6 and O_2 gases, respectively. The bias and inductively coupled plasma powers were 5 and 900 W, respectively, which could form the nanoscale black silicon patterns on the bottom trench surfaces.[65] The wafer was again introduced to piranha solution for 15 min, rinsed with deionized water, and dried in N_2 gas for 5 min. These samples were exposed to oxygen plasma for 10 min prior to coating.

As for the PDMS samples, the microstructured silicon wafer was first spin-coated with a thin (10 nm) layer of polytetrafluoroethylene (Teflon, DuPont, Wilmington, DE) conformally to make the surface hydrophobic. The hydrophobized silicon wafer was then used as a mold to replicate the micropatterns on to PDMS surfaces. Uncured PDMS and its cure agent were mixed (10:1, Dow-Corning, Sylgard-184) and the mixture was flow-coated over the silicon mold. After the flow-coating, the PDMS with the silicon mold was exposed to vacuum at room temperature

for 48 h to remove air cavities between them before it was fully cured. Afterwards, the PDMS layer was peeled off from the silicon mold, forming inverted structures of the silicon mold and cut into pieces to a desirable size.

Fabrication of Nano-patterned Silicon

Polished silicon wafers (University Wafer, Inc.) were cleaned in piranha solution, rinsed with deionized water, and dehydrated on a hotplate at 100°C for 10 min. A positive photoresist (PR1-2000A, Futurrex, Inc., Franklin, NJ) was spin-coated on a wafer for 40 s at 3000 rpm, resulting in a film thickness of 200 nm, and baked at 120°C for 2 min. A maskless laser interference lithography was used to define periodic nanopatterns.[66] A He–Cd laser (50 mW and 30 cm coherence length at a wavelength of 325 nm) was used in Lloyd's mirror setup for the interference lithography. A total dosage of 20 mJ/cm^2 was used for exposure. The wafers were then post-baked at 100°C for 1 min before being placed in an undiluted resist developer (RD6, Futurrex, Inc.) for 12 s. The developed patterns were rinsed with deionized water for 3 min and dried with N_2 gas. The photoresist patterns were then used as etch masks to transfer the periodic nanopatterns onto silicon wafers using a cryogenic DRIE process (PlasmaLab 100, Oxford Instruments, Bristol, UK) at -100°C using SF_6 and O_2 gases. The wafers were again introduced to piranha solution for 15 min, rinsed with deionized water, and dried in N_2 gas for 5 min. These samples were exposed to oxygen plasma for 10 min prior to coating.

Layer-by-Layer Deposition

To prepare for LbL deposition, silicon wafers were cut into 1 cm × 1 cm pieces, cleaned by overnight exposure to UV light, and soaked in a sulfuric acid bath for 40 min to clean and introduce charged groups to the surface, as described elsewhere.[67] Phosphate buffer (PB) washes

(0.01 M), polycation solutions (0.2 mg/mL in Milli-Q water), and anionic PPZ solutions (0.4 mg/mL in 0.01 M PB) were pH-adjusted by additions of 0.1 or 0.01 M NaOH or HCl. As described elsewhere,[68] substrates were primed with a monolayer of BPEI at pH 9 for 15 minutes and rinsed with PB at the pH selected for deposition conditions. Then, layers of PPZ and polycation were alternately deposited on the wafer by soaking in solutions at the same selected pH for 5 min, finally capping the film with a PPZ layer.

To demonstrate the versatility of these coatings, the multilayers were deposited following the same procedure on patterned silicon (synthesized as described in this paper), titanium sheets (Sigma-Aldrich), and glass. Deposition on patterned PDMS and fabrics followed a slightly modified procedure, omitting the exposure to UV light and sulfuric acid. PDMS wafers were prepared for deposition by sonicating in a 50% (v/v) ethanol/water mixture for 15 seconds, rather than plasma treating, to remove any remaining debris or contamination, then rinsing with Milli-Q water and drying with N_2 gas.

Spin-coating of Poly[bis(2,2,2-trifluoroethoxy)phosphazene] (PTFEP)

To prepare for spin-coating of poly[bis(2,2,2-trifluoroethoxy)phosphazene] (PTFEP) on silicon, silicon wafers were cut into 1 cm × 1 cm pieces and cleaned by exposure to UV light overnight. PTFEP was dissolved in acetone (1 mg/mL, ACS grade, VWR) and injected onto the wafer in 50 μL increments. The wafer was rotated at 1000 rpm for 2 min using a Laurell Technologies Corporation WS-650-23NNP/UD3/UD3B spin coater. The PTFEP solution was injected every 30 s to achieve films with ~40 nm thickness, as measured by spectroscopic ellipsometry.

Spectroscopic Ellipsometry

The thicknesses and refractive indices of the LbL films were characterized using a M-2000 automated-angle spectroscopic ellipsometer (J.A. Woollam Co., Inc.). Dry film measurements were collected at four incidence angles: 45°, 55°, 65°, and 75°. Liquid cell measurements, used to measure the swelling of the films, were collected at 75° until a constant swollen thickness was reached (~30 min). Prior to filling the cell with pH adjusted PB, the dry film thickness was measured in the cell for an accurate calculation of the swollen thickness.

To fit the ellipsometric data, the dry polymer film on the Si wafer was treated as a Cauchy material of thickness *d* atop a Si and native oxide layer. Wet-cell measurements of swollen polymer films required the addition of a fourth layer to the model to account for the refractive index of the solvent. Fitting coefficients and thickness *d* were fitted simultaneously as described previously.[44]

Contact Angle Goniometry

After deposition of the film, the wafers were rinsed with water and dried with nitrogen gas. Static contact angle measurements of 7 μL ultrapure water droplets were collected with a camera (The Imaging Source, LLC) on a CAM 101 setup (KSV Instruments Ltd.) and analyzed using OneAttension software. Measurements were averaged over three different locations on each wafer. Advancing and receding contact angle measurements were collected using a home-built apparatus for performing the volumetric drop method. The measurements were conducted in triplicate, and the determined advancing and receding angles were averaged.

Attenuated Total Reflection Fourier Transform Infrared (ATR-FTIR) Spectroscopy

A Bruker Tensor II spectrometer equipped with a mercury cadmium telluride detector and an ATR diamond crystal was used for collecting ATR-FTIR spectra. The spectra were accumulated by 96 scans in a spectral range of 900-4000 cm^{-1} at a resolution of 2 cm^{-1}.

To analyze the degree of ionization of the carboxylic acid groups within the films as a function of deposition solution pH, PVAm/FP77 films of ~100 nm dry thickness (FP77-capped) were deposited on undoped silicon wafers (University Wafer, Inc.) The films were dried with nitrogen gas, and the spectra were collected for the films. For peak identification, spectra of the FP77 and PVAm polyelectrolytes were acquired by depositing a monolayer on the ATR crystal by solution evaporation. The spectrum for FP77 was acquired while running a constant stream of nitrogen gas to inhibit the hygroscopic behavior of the polymer.

Atomic Force Microscopy

A Bruker Dimension Icon AFM was used to obtain images of the morphology of the PVAm/FP77 films. The samples were deposited on a silicon wafer either from varied deposition pH or with varied thickness to determine the effect on the film morphology. After deposition, the samples were rinsed with water and dried overnight. The imaging was conducted using a silicon cantilever with a normal stiffness of K_n= 7.4 N/m.

Durability Testing

To test the adhesion of the coating to the substrate, a 15-bilayer PVAm/FP77 coating was scratched with a razor in a crosshatch pattern as described by ASTM D3359. Pressure-sensitive tape was applied to the scratched area and removed at an angle parallel to the surface of the substrate. This procedure was repeated three times and imaged in the same area with an optical microscope after each tape removal.

To test solvent resistance, $(PVAm/FP77)_5$-coated silicon wafers were placed in a beaker filled with 20 mL of toluene, hexane, ethanol, methanol, or dimethyl sulfoxide for up to 12 hours. Contact angle and thickness measurements were taken before exposure, after 30 seconds of exposure, and after 12 hours of exposure. The wafers were rinsed with ultrapure water before taking contact angle measurements.

To test the stability under flowing water, $(PVAm/FP77)_5$-coated silicon wafers were held under a stream of tap water (30 mL/s) for up to 10 minutes. Contact angle and thickness measurements were taken before exposure and after 1 and 5 minutes of exposure. The wafer was allowed to dry before taking contact angle measurements.

Author Information

Corresponding Authors

Svetlana A. Sukhishvili – Department of Materials Science & Engineering, Texas A&M University, College Station, Texas 77843, United States; Email: svetlana@tamu.edu

Chang-Hwan Choi – Department of Mechanical Engineering, Stevens Institute of Technology, Hoboken, New Jersey 07030, United States; Email: cchoi@stevens.edu

Authors

Jordan Brito – Department of Materials Science & Engineering, Texas A&M University, College Station, Texas 77843, United States

Kaustubh Asawa – Department of Mechanical Engineering, Stevens Institute of Technology, Hoboken, New Jersey 07030, United States

Alexander Marin – Institute for Bioscience and Biotechnology Research, University of Maryland, Rockville, Maryland 20853, United States

Alexander K. Andrianov – Institute for Bioscience and Biotechnology Research, University of Maryland, Rockville, Maryland 20853, United States

Notes

The authors declare no competing financial interest.

Supporting Information

The Supporting Information is available free of charge at:

(PDF) Ellipsometric thicknesses, RMS roughness, 2D surface projections, and static contact angles for 5-bilayer films with varying degree of fluorination, polyamine binding partner, or deposition pH; temporal change in static contact angle for coatings with varying polyamine binding partner; an example calculation of carboxyl ionization degree from an ATR-FTIR spectrum; ATR-FTIR spectra and ionization degree of FP77 in solutions of different pH; thicknesses, ratios, and schematics for pH-dependent adsorbed layers; 2D surface projections and SEM images of PVAm/FP77 films with varying amounts of bilayers; thickness-dependent static contact angle for BPEI/FP77; SEM and optical images of nano-pillared silicon and its dependence of contact angle on coating thickness; apparent contact angles and contact angle hysteresis for $(PVAm/FP77)_5$ films on grooved silicon, $\varphi = 0.5$; optical images of microstructured PDMS and PDMS before and after dying with Rhodamine 5G; optical images of tape test results; and change in thickness and contact angle of $(PVAm/FP77)_5$ after exposure to solvents and a jet of water.

Videos S1 & S2. Videos showing successful and failed droplet transfer on coated, grooved silicon substrates, respectively (MP4).

Video S3. Video showing pH-selective droplet transfer between coated, grooved silicon substrates (MP4).

Videos S4 & S5. Video showing successful and failed droplet transfer on coated, grooved PDMS substrates, respectively (MP4).

Video S6. Video demonstrating a reaction-in-a-droplet enabled by coated, grooved PDMS substrates (MP4).

Acknowledgments

This work was supported in part by the National Science Foundation under Award DMR-1808483 (S.S.), CMMI-1537474 (C.C.), and DMR-1808531 (A.A.). J.B. acknowledges financial support from the Texas A&M University Graduate Diversity Excellence Fellowship, National Science Foundation Graduate Research Fellowship Program, and Texas A&M Engineering Experiment Station (TEES). Authors are grateful to Qing Zhou for conducting AFM imaging, Zhen Sang for conducting additional SEM imaging, and undergraduate researchers Molly Guyette, Lauren Wilkin, Noah Sharp, and Isabella Alvarado for help with sample preparation. Use of the Materials Characterization Facility at Texas A&M University is acknowledged.

References

(1) Li, H.; Li, A.; Zhao, Z.; Xue, L.; Li, M.; Song, Y. Precise Droplet Manipulation Based on Surface Heterogeneity. *Acc. Mater. Res.* **2021**, *2* (4), 230–241. https://doi.org/10.1021/accountsmr.1c00005.

(2) Lehmann, U.; Vandevyver, C.; Parashar, V. K.; Gijs, M. A. M. Droplet-Based DNA Purification in a Magnetic Lab-on-a-Chip. *Angew. Chem. Int. Ed.* **2006**, *45* (19), 3062–3067. https://doi.org/10.1002/anie.200503624.

(3) Yao, X.; Song, Y.; Jiang, L. Applications of Bio-Inspired Special Wettable Surfaces. *Adv. Mater.* **2011**, *23* (6), 719–734. https://doi.org/10.1002/adma.201002689.

(4) Tang, X.; Zhu, P.; Tian, Y.; Zhou, X.; Kong, T.; Wang, L. Mechano-Regulated Surface for Manipulating Liquid Droplets. *Nat. Commun.* **2017**, *8* (1), 14831. https://doi.org/10.1038/ncomms14831.

(5) Yang, Z.; Wei, J.; Sobolev, Y. I.; Grzybowski, B. A. Systems of Mechanized and Reactive Droplets Powered by Multi-Responsive Surfactants. *Nature* **2018**, *553* (7688), 313–318. https://doi.org/10.1038/nature25137.

(6) Xing, Y.; Shang, W.; Wang, Q.; Feng, S.; Hou, Y.; Zheng, Y. Integrative Bioinspired Surface with Wettable Patterns and Gradient for Enhancement of Fog Collection. *ACS Appl. Mater. Interfaces* **2019**, *11* (11), 10951–10958. https://doi.org/10.1021/acsami.8b19574.

(7) Sun, L.; Bian, F.; Wang, Y.; Wang, Y.; Zhang, X.; Zhao, Y. Bioinspired Programmable Wettability Arrays for Droplets Manipulation. *Proc. Natl. Acad. Sci.* **2020**, *117* (9), 4527–4532. https://doi.org/10.1073/pnas.1921281117.

(8) Li, Y.; He, L.; Zhang, X.; Zhang, N.; Tian, D. External-Field-Induced Gradient Wetting for Controllable Liquid Transport: From Movement on the Surface to Penetration into the Surface. *Adv. Mater.* **2017**, *29* (45), 1703802. https://doi.org/10.1002/adma.201703802.

(9) Huang, G.; Li, M.; Yang, Q.; Li, Y.; Liu, H.; Yang, H.; Xu, F. Magnetically Actuated Droplet Manipulation and Its Potential Biomedical Applications. *ACS Appl. Mater. Interfaces* **2017**, *9* (2), 1155–1166. https://doi.org/10.1021/acsami.6b09017.

(10) Irajizad, P.; Ray, S.; Farokhnia, N.; Hasnain, M.; Baldelli, S.; Ghasemi, H. Remote Droplet Manipulation on Self-Healing Thermally Activated Magnetic Slippery Surfaces. *Adv. Mater. Interfaces* **2017**, *4* (12), 1700009. https://doi.org/10.1002/admi.201700009.

(11) Li, A.; Li, H.; Li, Z.; Zhao, Z.; Li, K.; Li, M.; Song, Y. Programmable Droplet Manipulation by a Magnetic-Actuated Robot. *Sci. Adv.* **2020**, *6* (7), eaay5808. https://doi.org/10.1126/sciadv.aay5808.

(12) Sung Kwon Cho; Hyejin Moon; Chang-Jin Kim. Creating, Transporting, Cutting, and Merging Liquid Droplets by Electrowetting-Based Actuation for Digital Microfluidic Circuits. *J. Microelectromechanical Syst.* **2003**, *12* (1), 70–80. https://doi.org/10.1109/JMEMS.2002.807467.

(13) Teng, P.; Tian, D.; Fu, H.; Wang, S. Recent Progress of Electrowetting for Droplet Manipulation: From Wetting to Superwetting Systems. *Mater. Chem. Front.* **2020**, *4* (1), 140–154. https://doi.org/10.1039/C9QM00458K.

(14) Phan, H. V.; Alan, T.; Neild, A. Droplet Manipulation Using Acoustic Streaming Induced by a Vibrating Membrane. *Anal. Chem.* **2016**, *88* (11), 5696–5703. https://doi.org/10.1021/acs.analchem.5b04481.

(15) Zhang, S. P.; Lata, J.; Chen, C.; Mai, J.; Guo, F.; Tian, Z.; Ren, L.; Mao, Z.; Huang, P.-H.; Li, P.; Yang, S.; Huang, T. J. Digital Acoustofluidics Enables Contactless and Programmable Liquid Handling. *Nat. Commun.* **2018**, *9* (1), 2928. https://doi.org/10.1038/s41467-018-05297-z.
(16) Baigl, D. Photo-Actuation of Liquids for Light-Driven Microfluidics: State of the Art and Perspectives. *Lab. Chip* **2012**, *12* (19), 3637–3653. https://doi.org/10.1039/C2LC40596B.
(17) Gao, C.; Wang, L.; Lin, Y.; Li, J.; Liu, Y.; Li, X.; Feng, S.; Zheng, Y. Droplets Manipulated on Photothermal Organogel Surfaces. *Adv. Funct. Mater.* **2018**, *28* (35), 1803072. https://doi.org/10.1002/adfm.201803072.
(18) Liu, Y.; Zhu, C.; Zhao, Y.; Qing, X.; Wang, F.; Deng, D.; Wei, J.; Yu, Y. Directed Pinning of Moving Water Droplets on Photoresponsive Liquid Crystal Mats. *Adv. Mater. Interfaces* **2019**, *6* (21), 1901158. https://doi.org/10.1002/admi.201901158.
(19) Jiang, Y.; Wang, Z.; Yu, X.; Shi, F.; Xu, H.; Zhang, X.; Smet, M.; Dehaen, W. Self-Assembled Monolayers of Dendron Thiols for Electrodeposition of Gold Nanostructures: Toward Fabrication of Superhydrophobic/Superhydrophilic Surfaces and pH-Responsive Surfaces. *Langmuir* **2005**, *21* (5), 1986–1990. https://doi.org/10.1021/la047491b.
(20) Yu, X.; Wang, Z.; Jiang, Y.; Shi, F.; Zhang, X. Reversible pH-Responsive Surface: From Superhydrophobicity to Superhydrophilicity. *Adv. Mater.* **2005**, *17* (10), 1289–1293. https://doi.org/10.1002/adma.200401646.
(21) Xia, F.; Feng, L.; Wang, S.; Sun, T.; Song, W.; Jiang, W.; Jiang, L. Dual-Responsive Surfaces That Switch between Superhydrophilicity and Superhydrophobicity. *Adv. Mater.* **2006**, *18* (4), 432–436. https://doi.org/10.1002/adma.200501772.
(22) Jiang, Y.; Wan, P.; Smet, M.; Wang, Z.; Zhang, X. Self-Assembled Monolayers of a Malachite Green Derivative: Surfaces with pH- and UV-Responsive Wetting Properties. *Adv. Mater.* **2008**, *20* (10), 1972–1977. https://doi.org/10.1002/adma.200702366.
(23) Liu, X.; Ye, Q.; Yu, B.; Liang, Y.; Liu, W.; Zhou, F. Switching Water Droplet Adhesion Using Responsive Polymer Brushes. *Langmuir* **2010**, *26* (14), 12377–12382. https://doi.org/10.1021/la101909e.
(24) Cheng, Z.; Du, M.; Lai, H.; Du, Y.; Zhang, N.; Sun, K. Selective Transportation of Microdroplets Assisted by a Superhydrophobic Surface with pH-Responsive Adhesion. *Chem. – Asian J.* **2013**, *8* (12), 3200–3206. https://doi.org/10.1002/asia.201300941.
(25) Nascimento, J. U.; Zambuzi, G. C.; Ferreira, J. O.; Paula, J. H.; Ribeiro, T. S.; Souza, A. L.; Dreiss, C. A.; Silva, L. L.; Francisco, K. R. A Simple Process to Tune Wettability of Pectin-Modified Silanized Glass. *Colloids Surf. Physicochem. Eng. Asp.* **2019**, *577*, 67–74. https://doi.org/10.1016/j.colsurfa.2019.05.056.
(26) Guo, S.; Zhu, X.; Li, M.; Shi, L.; Ong, J. L. T.; Jańczewski, D.; Neoh, K. G. Parallel Control over Surface Charge and Wettability Using Polyelectrolyte Architecture: Effect on Protein Adsorption and Cell Adhesion. *ACS Appl. Mater. Interfaces* **2016**, *8* (44), 30552–30563. https://doi.org/10.1021/acsami.6b09481.
(27) Lin, C.-H.; Cho, H.-L.; Yeh, Y.-H.; Yang, M.-C. Improvement of the Surface Wettability of Silicone Hydrogel Contact Lenses via Layer-by-Layer Self-Assembly Technique. *Colloids Surf. B Biointerfaces* **2015**, *136*, 735–743. https://doi.org/10.1016/j.colsurfb.2015.10.006.
(28) Han, J. T.; Zheng, Y.; Cho, J. H.; Xu, X.; Cho, K. Stable Superhydrophobic Organic−Inorganic Hybrid Films by Electrostatic Self-Assembly. *J. Phys. Chem. B* **2005**, *109* (44), 20773–20778. https://doi.org/10.1021/jp052691x.

(29) Yoo, D.; Shiratori, S. S.; Rubner, M. F. Controlling Bilayer Composition and Surface Wettability of Sequentially Adsorbed Multilayers of Weak Polyelectrolytes. *Macromolecules* **1998**, *31* (13), 4309–4318. https://doi.org/10.1021/ma9800360.
(30) Elzbieciak, M.; Kolasinska, M.; Warszynski, P. Characteristics of Polyelectrolyte Multilayers: The Effect of Polyion Charge on Thickness and Wetting Properties. *Colloids Surf. Physicochem. Eng. Asp.* **2008**, *321* (1), 258–261. https://doi.org/10.1016/j.colsurfa.2008.01.036.
(31) Kolasińska, M.; Warszyński, P. The Effect of Nature of Polyions and Treatment after Deposition on Wetting Characteristics of Polyelectrolyte Multilayers. *Appl. Surf. Sci.* **2005**, *252* (3), 759–765. https://doi.org/10.1016/j.apsusc.2005.02.060.
(32) Kolasińska, M.; Warszyński, P. The Effect of Support Material and Conditioning on Wettability of PAH/PSS Multilayer Films. *Bioelectrochemistry* **2005**, *66* (1), 65–70. https://doi.org/10.1016/j.bioelechem.2004.03.009.
(33) Steitz, R.; Jaeger, W.; Klitzing, R. v. Influence of Charge Density and Ionic Strength on the Multilayer Formation of Strong Polyelectrolytes. *Langmuir* **2001**, *17* (15), 4471–4474. https://doi.org/10.1021/la010168d.
(34) Glinel, K.; Moussa, A.; Jonas, A. M.; Laschewsky, A. Influence of Polyelectrolyte Charge Density on the Formation of Multilayers of Strong Polyelectrolytes at Low Ionic Strength. *Langmuir* **2002**, *18* (4), 1408–1412. https://doi.org/10.1021/la0113670.
(35) Tang, K.; Besseling, N. A. M. Formation of Polyelectrolyte Multilayers: Ionic Strengths and Growth Regimes. *Soft Matter* **2016**, *12* (4), 1032–1040. https://doi.org/10.1039/C5SM02118A.
(36) Xu, L.; Ankner, J. F.; Sukhishvili, S. A. Steric Effects in Ionic Pairing and Polyelectrolyte Interdiffusion within Multilayered Films: A Neutron Reflectometry Study. *Macromolecules* **2011**, *44* (16), 6518–6524. https://doi.org/10.1021/ma200986d.
(37) Shiratori, S. S.; Rubner, M. F. pH-Dependent Thickness Behavior of Sequentially Adsorbed Layers of Weak Polyelectrolytes. *Macromolecules* **2000**, *33* (11), 4213–4219. https://doi.org/10.1021/ma991645q.
(38) Bieker, P.; Schönhoff, M. Linear and Exponential Growth Regimes of Multilayers of Weak Polyelectrolytes in Dependence on pH. *Macromolecules* **2010**, *43* (11), 5052–5059. https://doi.org/10.1021/ma1007489.
(39) Kaur, J.; Kaur, G. Optimization of pH Conditions and Characterization of Polyelectrolyte Complexes between Gellan Gum and Cationic Guar Gum. *Polym. Adv. Technol.* **2018**, *29* (12), 3035–3048. https://doi.org/10.1002/pat.4424.
(40) Zhai, L.; Cebeci, F. Ç.; Cohen, R. E.; Rubner, M. F. Stable Superhydrophobic Coatings from Polyelectrolyte Multilayers. *Nano Lett.* **2004**, *4* (7), 1349–1353. https://doi.org/10.1021/nl049463j.
(41) Jisr, R. M.; Rmaile, H. H.; Schlenoff, J. B. Hydrophobic and Ultrahydrophobic Multilayer Thin Films from Perfluorinated Polyelectrolytes. *Angew. Chem. Int. Ed.* **2005**, *44* (5), 782–785. https://doi.org/10.1002/anie.200461645.
(42) Soeno, T.; Inokuchi, K.; Shiratori, S. Ultra-Water-Repellent Surface: Fabrication of Complicated Structure of SiO2 Nanoparticles by Electrostatic Self-Assembled Films. *Appl. Surf. Sci.* **2004**, *237* (1), 539–543. https://doi.org/10.1016/j.apsusc.2004.06.041.
(43) Andrianov, A. K.; Marin, A.; Peterson, P.; Chen, J. Fluorinated Polyphosphazene Polyelectrolytes. *J. Appl. Polym. Sci.* **2007**, *103* (1), 53–58. https://doi.org/10.1002/app.23963.

(44) Selin, V.; Albright, V.; Ankner, J. F.; Marin, A.; Andrianov, A. K.; Sukhishvili, S. A. Biocompatible Nanocoatings of Fluorinated Polyphosphazenes through Aqueous Assembly. *ACS Appl. Mater. Interfaces* **2018**, *10* (11), 9756–9764. https://doi.org/10.1021/acsami.8b02072.
(45) Albright, V.; Marin, A.; Kaner, P.; Sukhishvili, S. A.; Andrianov, A. K. New Family of Water-Soluble Sulfo–Fluoro Polyphosphazenes and Their Assembly within Hemocompatible Nanocoatings. *ACS Appl. Bio Mater.* **2019**, acsabm.9b00485. https://doi.org/10.1021/acsabm.9b00485.
(46) Albright, V.; Penarete-Acosta, D.; Stack, M.; Zheng, J.; Marin, A.; Hlushko, H.; Wang, H.; Jayaraman, A.; Andrianov, A. K.; Sukhishvili, S. A. Polyphosphazenes Enable Durable, Hemocompatible, Highly Efficient Antibacterial Coatings. *Biomaterials* **2021**, *268*, 120586. https://doi.org/10.1016/j.biomaterials.2020.120586.
(47) Bayer, I. S. Superhydrophobic Coatings from Ecofriendly Materials and Processes: A Review. *Adv. Mater. Interfaces* **2020**, *7* (13), 2000095. https://doi.org/10.1002/admi.202000095.
(48) Hougham, G.; Tesoro, G.; Viehbeck, A. Influence of Free Volume Change on the Relative Permittivity and Refractive Index in Fluoropolyimides. *Macromolecules* **1996**, *29* (10), 3453–3456. https://doi.org/10.1021/ma9503423.
(49) Albright, V.; Selin, V.; Hlushko, H.; Palanisamy, A.; Marin, A.; Andrianov, A. K.; Sukhishvili, S. A. Fluorinated Polyphosphazene Coatings Using Aqueous Nano-Assembly of Polyphosphazene Polyelectrolytes. In *Polyphosphazenes in Biomedicine, Engineering, and Pioneering Synthesis*; ACS Symposium Series; American Chemical Society, 2018; Vol. 1298, pp 101–118. https://doi.org/10.1021/bk-2018-1298.ch005.
(50) Fu, J.; Fares, H. M.; Schlenoff, J. B. Ion-Pairing Strength in Polyelectrolyte Complexes. *Macromolecules* **2017**, *50* (3), 1066–1074. https://doi.org/10.1021/acs.macromol.6b02445.
(51) Sukhishvili, S. A.; Kharlampieva, E.; Izumrudov, V. Where Polyelectrolyte Multilayers and Polyelectrolyte Complexes Meet. *Macromolecules* **2006**, *39* (26), 8873–8881. https://doi.org/10.1021/ma061617p.
(52) Nazaran, P.; Bosio, V.; Jaeger, W.; Anghel, D. F.; v. Klitzing, R. Lateral Mobility of Polyelectrolyte Chains in Multilayers. *J. Phys. Chem. B* **2007**, *111* (29), 8572–8581. https://doi.org/10.1021/jp068768e.
(53) Guazzelli, E.; Galli, G.; Martinelli, E. The Effect of Poly(Ethylene Glycol) (PEG) Length on the Wettability and Surface Chemistry of PEG-Fluoroalkyl-Modified Polystyrene Diblock Copolymers and Their Two-Layer Films with Elastomer Matrix. *Polymers* **2020**, *12* (6), 1236. https://doi.org/10.3390/polym12061236.
(54) Chen, J.; Luo, G.; Cao, W. The Study of Layer-by-Layer Ultrathin Films by the Dynamic Contact Angle Method. *J. Colloid Interface Sci.* **2001**, *238* (1), 62–69. https://doi.org/10.1006/jcis.2001.7460.
(55) Singh, A.; Steely, L.; Allcock, H. R. Poly[Bis(2,2,2-Trifluoroethoxy)Phosphazene] Superhydrophobic Nanofibers. *Langmuir* **2005**, *21* (25), 11604–11607. https://doi.org/10.1021/la052110v.
(56) Wenzel, R. N. Resistance of Solid Surfaces to Wetting by Water. *Ind. Eng. Chem.* **1936**, *28* (8), 988–994. https://doi.org/10.1021/ie50320a024.
(57) Burke, S. E.; Barrett, C. J. Acid−Base Equilibria of Weak Polyelectrolytes in Multilayer Thin Films. *Langmuir* **2003**, *19* (8), 3297–3303. https://doi.org/10.1021/la026500i.

(58) Kharlampieva, E.; Sukhishvili, S. A. Ionization and pH Stability of Multilayers Formed by Self-Assembly of Weak Polyelectrolytes. *Langmuir* **2003**, *19* (4), 1235–1243. https://doi.org/10.1021/la026546b.
(59) Marin, A.; Brito, J.; Sukhishvili, S. A.; Andrianov, A. K. Cationic Fluoropolyphosphazenes: Synthesis and Assembly with Heparin as a Pathway to Hemocompatible Nanocoatings. *ACS Appl. Bio Mater.* **2022**, *5* (1), 313–321. https://doi.org/10.1021/acsabm.1c01099.
(60) Cassie, A. B. D.; Baxter, S. Wettability of Porous Surfaces. *Trans. Faraday Soc.* **1944**, *40* (0), 546–551. https://doi.org/10.1039/TF9444000546.
(61) Jiang, Y.; Choi, C.-H. Droplet Retention on Superhydrophobic Surfaces: A Critical Review. *Adv. Mater. Interfaces* **2021**, *8* (2), 2001205. https://doi.org/10.1002/admi.202001205.
(62) Lu, Y.; Sarshar, M. A.; Du, K.; Chou, T.; Choi, C.-H.; Sukhishvili, S. A. Large-Amplitude, Reversible, pH-Triggered Wetting Transitions Enabled by Layer-by-Layer Films. *ACS Appl. Mater. Interfaces* **2013**, *5* (23), 12617–12623. https://doi.org/10.1021/am403944m.
(63) Holmes-Farley, S. R.; Reamey, R. H.; McCarthy, T. J.; Deutch, J.; Whitesides, G. M. Acid-Base Behavior of Carboxylic Acid Groups Covalently Attached at the Surface of Polyethylene: The Usefulness of Contact Angle in Following the Ionization of Surface Functionality. *Langmuir* **1985**, *1* (6), 725-740. https://doi.org/10.1021/la00066a016.
(64) Andrianov, A. K.; Svirkin, Y. Y.; LeGolvan, M. P. Synthesis and Biologically Relevant Properties of Polyphosphazene Polyacids. *Biomacromolecules* **2004**, *5* (5), 1999–2006. https://doi.org/10.1021/bm049745d.
(65) Jansen, H.; Boer, M. de; Legtenberg, R.; Elwenspoek, M. The Black Silicon Method: A Universal Method for Determining the Parameter Setting of a Fluorine-Based Reactive Ion Etcher in Deep Silicon Trench Etching with Profile Control. *J. Micromech. Microeng.* **1995**, *5* (2), 115–120. https://doi.org/10.1088/0960-1317/5/2/015.
(66) Wathuthanthri, I.; Liu, Y.; Du, K.; Xu, W.; Choi, C.-H. Simple Holographic Patterning for High-Aspect-Ratio Three-Dimensional Nanostructures with Large Coverage Area. *Adv. Funct. Mater.* **2013**, *23* (5), 608–618. https://doi.org/10.1002/adfm.201201814.
(67) Dubas, S. T.; Schlenoff, J. B. Factors Controlling the Growth of Polyelectrolyte Multilayers. *Macromolecules* **1999**, *32* (24), 8153–8160. https://doi.org/10.1021/ma981927a.
(68) Kozlovskaya, V.; Yakovlev, S.; Libera, M.; Sukhishvili, S. A. Surface Priming and the Self-Assembly of Hydrogen-Bonded Multilayer Capsules and Films. *Macromolecules* **2005**, *38* (11), 4828–4836. https://doi.org/10.1021/ma0501895.

Table of Content Figure

Hierarchically Structured, All-Aqueous-Coated Hydrophobic Surfaces with pH-Selective Droplet Transfer Capability

Jordan Brito[1], Kaustubh Asawa[2], Alexander Marin,[3] Alexander K. Andrianov,[3] Chang-Hwan Choi[2], and Svetlana A. Sukhishvili[1]**

[1]Department of Materials Science & Engineering, Texas A&M University, College Station, TX 77843, USA

[2]Department of Mechanical Engineering, Stevens Institute of Technology, Hoboken, NJ 07030, USA

[3]Institute for Bioscience and Biotechnology Research, University of Maryland, Rockville, MD 20850, USA